NIH Public Access
Author Manuscript
Chemphyschem. Author manuscript; available in PMC 2014 March 27.

Published in final edited form as:
Chemphyschem. 2014 March 17; 15(4): 687–695. doi:10.1002/cphc.201300757.

Localization microscopy using noncovalent fluorogen activation by genetically encoded fluorogen activating proteins

Qi Yan[#1,2], **Samantha L. Schwartz**[#3], **Suvrajit Maji**[1,4], **Fang Huang**[5], **Chris Szent-Gyorgyi**[1], **Diane S. Lidke**[3], **Keith A. Lidke**[5], and **Marcel P. Bruchez**[1,2,4,6,*]

[1]Molecular Biosensor and Imaging Center, Carnegie Mellon Unviersity, Pittsburgh PA 15213

[2]Department of Biological Sciences, Carnegie Mellon University, Pittsburgh, PA 15213

[3]Department of Pathology and Cancer Research and Treatment Center, University of New Mexico, Albuquerque, NM 87131

[4]Lane Center for Computational Biology, Carnegie Mellon University, Pittsburgh, PA 15213

[5]Department of Physics, University of New Mexico, Albuquerque, NM 87131

[6]Department of Chemistry, Carnegie Mellon University, Pittsburgh, PA 15213

[#] These authors contributed equally to this work.

Abstract

The noncovalent equilibrium activation of a fluorogenic malachite green dye and its cognate fluorogen activating protein has been exploited to produce a sparse labeling distribution of densely tagged genetically encoded proteins, enabling single molecule detection and superresolution imaging in fixed and living cells. These sparse labeling conditions are achieved by control of the dye concentration in the milieu, and do not require any photoswitching or photoactivation. The labeling is achieved using physiological buffers and cellular media, and does not require additives or switching buffer to obtain superresolution images. We evaluate superresolution properties and images obtained from a selected fluorogen activating protein clone fused to actin, and show that the photon counts per object fall between those typically reported for fluorescent proteins and switching dye-pairs, resulting in 10-30 nm localization precision per object. This labeling strategy complements existing approaches, and may simplify multicolor labeling of cellular structures.

Keywords

Superresolution; Localization; Live Cell; Fluorescent Protein; Fluorescence; Imaging

Introduction

The resolution of conventional fluorescence microscopy is at least an order of magnitude poorer than the desired resolution in biological specimens. A single emitting dye molecule, typically 1-2 nm in size, produces a fluorescent image that is 100-fold larger, with a diffraction limited point-spread function that is >200 nm full-width at half-maximum. Objects nearer than this cannot be resolved, resulting in “blurred” images that obscure the true positions of the underlying molecules. The result is that many molecular structures cannot be adequately visualized in the crowded environment of the cell because their locations are not resolvable under the microscope. Over the past decade, a number of

[*]To whom correspondence should be addressed bruchez@cmu.edu.

NIH-PA Author Manuscript
NIH-PA Author Manuscript
NIH-PA Author Manuscript

NIH-PA Author Manuscript

NIH-PA Author Manuscript

NIH-PA Author Manuscript

approaches to overcome these limits have been applied to biological specimens, revealing structural features and biological processes that were beyond the reach of previous fluorescent imaging approaches.[1]

To circumvent the diffraction limit in widefield microscopy, two general methods have been employed: structuring the pattern of emitting molecules or randomly sampling a sparse subset of the emitting molecules. In the structured methods, emitters are confined to regions with spatial frequencies greater than the diffraction limit, either by image combination (in the case of so-called Structured Illumination Microscopy (SIM)),[2-4] or by overlapping laser illumination spots that manipulate the electronic states of the emitters (confining emitters to a smaller spot than the diffraction limit in the case of Stimulated Emission Depletion Microscopy).[5, 6] These methods substantially extend the resolution of conventional microscopy, typically by a factor of 2-3-fold, although new probes with optimized properties may provide significantly improved resolution beyond these levels.[7]

The random sampling of a sparse subset of fluorescent labels in a specimen has proven to be easier to implement in a variety of instruments and cellular contexts,[8-11] primarily because many conventional labels have been shown to function as intermittent probes in a suitable environment.[12, 13] In this approach, individual resolvable fluorophores are activated within an image area from a pool of many “dark” molecules. These individual objects are spatially separated and provide discrete fluorescent points, allowing computational analysis to find the “center” position of the underlying molecule. Many cycles of imaging, bleaching, and photoactivation of a new subset of emitters produces an image series in which the majority of emitters have been activated at least once, and these can then be analyzed to find the set of positions. The map of positions from this time series, after correction for any drift in the image, represents a high-resolution view of the structure of interest.

This stochastic sampling approach was nearly simultaneously reported using three distinct labeling approaches. Photoactivatable fluorescent proteins were used as genetically encoded reporters for specific subcellular structures in fixed cells (PhotoActivation Localization Microscopy: PALM, F-PALM);[9, 10] cyanine dye pairs were used as a reversible photoswitchable tag to stain antibody labeled cellular structures (STochastic Optical Reconstruction Microscopy: STORM);[11] and fluorogenic lipid probes were shown to activate upon association with membrane structures (Point Accumulation Imaging of Nanoscale Topography: PAINT).[14] While the initial demonstrations of these imaging approaches were in thin sections in fixed cells under planar imaging conditions (TIRF or highly inclined illumination), the methods were rapidly extended to 3-d,[15-18] living cells[19] and multi-color labeling.[20, 21] Recent computational advances have allowed analysis of image fluctuation[22, 23] or photobleaching and blinking[24] data to extract superresolution information from significantly simplified acquisition protocols.

Labeling of proteins for sparse localization imaging was aided significantly with the recognition that many dyes undergo stochastic blinking in suitable buffers at timescales that are compatible with imaging.[12, 25, 26] These direct-STORM (d-STORM) approaches have allowed investigations with readily available antibody conjugates, and were also applied to genetically encoded targets using ligand-targeting[27] and chemical tagging approaches,[28] exploiting the intracellular environment to regulate switching. Each of these approaches, however, required targeting of intrinsically fluorescent dyes, potentially creating background issues and requiring acute labeling and washout of unbound dye or incomplete labeling of target sites.

Building on the initial PAINT methodology, it was recognized the fluorogenic probes would be desirable labels for cellular structures and specific molecules. DNA intercalating dyes

NIH-PA Author Manuscript

NIH-PA Author Manuscript

NIH-PA Author Manuscript

were used to visualize nucleic acid structures under random low-density binding and activation events,[29] an approach termed Binding and Activation Localization Microscopy (BALM). This approach was extended to enable fluorogenic labeling of heterogeneous catalysis reaction centers [30, 31], enzymatic activation[32] and toxin-labeling of ion channels.[33] In a related approach, binding of Cu(II) to a chelator positioned near a fluorescent dye resulted in a chemically reversible quenching that was tuned by the concentration of the exogenous copper ion. This approach was used to label tubulin in fixed, permeabilized antibody-labeled cells.[34] These approaches revealed a number of advantages for chemically-mediated, as opposed to photon-mediated switching: the approach is very simple to implement on a conventional fluorescence microscope, employing only a single laser;[30] excitation and switching are uncoupled, excitation power can be used to control localization rate while the chemical environment controls the switching rate for each dye; [34] there is reduced potential for phototoxicity; fluorescent activation by chemical or enzymatic means removes the requirement for probe wash-out.[32] While each of these approaches were useful in the targeted studies, general methods for fluorogenic labeling of target proteins, especially in living cells are not yet available.[35]

Fluorogen Activating Proteins as Genetically Encoded Tags

Recent work in our lab and others has established a family of proteins that activate the fluorescence of otherwise non-fluorescent dye molecules.[36] The first examples of these proteins (termed fluorogen activating proteins—FAPs) are based on single-chain variable fragment antibodies with specific molecular recognition properties for their cognate dyes (fluorogens). Binding of the dyes results in significant enhancements in extinction coefficient and fluorescence quantum yield, based on structural restriction of rotations around double bonds, but is fully reversible. Unbound dye, even previously bound, is essentially non-fluorescent. These fluorogen activating proteins have been fused to a variety of extracellular target proteins (including receptors,[37] ion channels[38, 39] and transporters), and recently optimized proteins have been expressed linked to intracellular proteins such as actin.[40, 41] The properties of the fluorescent complex can be tuned by directed evolution (random mutation and selection of proteins with improved properties),[42, 43] or by refinement of the properties of the fluorogen to produce improvements in brightness and/or affinity.[42] Both weak and tight-binding FAPs with high fluorescence quantum yield have been isolated, indicating that fluorescence is not tightly coupled to affinity.[44]

The malachite green chromophore is efficiently quenched in the excited state through a twisted intramolecular charge transfer process. This far-red absorbing dye molecule displays enhanced fluorescence in viscous solvents and low-temperature glasses. In addition, at higher concentrations, the dye shows binding and enhanced fluorescence with some endogenous proteins such as BSA. Of the fluorogens that we have evaluated, this dye shows the highest extinction coefficient (ε=110,000 $M^{-1}cm^{-1}$) bound to the protein, and displays molecular brightness in line with the brightest available fluorescent proteins. The MG dye is spectrally similar to Cy5, allowing robust single molecule detection with limited cellular autofluorescence. This dye, modified with either an ethyl ester or diethyleneglycol amine, binds to the same expressed FAP proteins with identical spectral properties, but is cell permeant only in the ester form.[45, 46]

We previously showed that MG-binding fluorogen activating protein-fluorogen complexes were compatible with STED microscopy,[40] producing image resolution comparable to the best available dye labels. These probes could be used to label genetically encoded proteins at the cell surface (membrane anchored, cell wall anchored, and receptors) or in the cytoplasm (actin). In this work, we sought to extend the superresolution imaging utility of these FAP-

NIH-PA Author Manuscript

NIH-PA Author Manuscript

NIH-PA Author Manuscript

fluorogen complexes to stochastic optical imaging by controlling the density of labeled objects with equilibrium binding.

Principles of Equilibrium Binding

The fractional occupancy of any receptor-ligand pair can be controlled using equilibrium principles. Single-site, non-cooperative interactions between a FAP and the fluorogen can be effectively modeled as a hyperbolic binding curve, where the fraction of binding sites occupied can be expressed in terms of the concentration of free dye and the solution K_D:

$$\theta = \frac{[dye]}{K_D + [dye]}$$

Under these conditions, half of the receptor sites are occupied when the concentration of free dye is equal to the K_D for the interaction. To achieve saturated labeling, concentrations considerably higher than the K_D are used. At concentrations lower than the interaction K_D, the fractional occupancy may be arbitrarily tuned to a low value, and this can be empirically optimized for a particular target protein, in order to achieve a sparse labeling pattern (Figure 1). In general, lower affinity clones may more readily release bound dyes, which would result in more rapid responses to changes in the concentration of free dye in solution.

If we consider the case of no photobleaching, we can understand the basic principle of this equilibrium approach to localization microscopy. Unbound dye is non-fluorescent, so at equilibrium a small fraction of receptors are binding and activating dye in any time window, while an equivalent number that are already bound are de-activated by dissociation. The pool of active molecules is thus held at a constant level, which can be tuned to a higher or lower density by increases or decreases in the bath concentration of free dye, respectively. Over time, all receptor sites are stochastically labeled, and the positions of each molecule can be found by localization.

Of course, real systems are not perfectly photostable, so it is important to consider the impact of photobleaching on these results. Once bound, the dye becomes fluorescent. In this state, for the purposes of localization imaging there are two relevant timescales to consider: dissociation and bleaching. The dye-protein complex will have a characteristic dissociation half-life for binding (in the absence of fluorescence excitation), and a characteristic bleaching rate. Because of chemical changes that occur in the bound dye-protein complex upon photobleaching, these parameters may be interdependent (i.e. the bleached complex may have a distinct dissociation timescale compared to the unbleached dye). We are analyzing a number of clones for these properties, but a detailed discussion is beyond the scope of this manuscript. The malachite green binding clones examined in this manuscript show bleaching prior to dissociation, and do not show any evidence of subsequent reactivation of bleached FAP-fluorogen complexes on the timescale of imaging. These relative timescales are an important area for future improvements of this labeling system for superresolution imaging.

Fluorogen activating proteins can be expressed as genetic fusions to targets of interest within living cells. While generally well tolerated, the presence of a genetically fused label can perturb the incorporation of the expressed protein within cellular structures, regardless of the type of label.[47] In the case of fluorogen activating proteins, and equilibrium localization, the dye must also access the target site at a controllable concentration. In some cellular compartments, accumulation of charged dyes may lead to levels of dye considerably higher or lower than that added to the bath.[48] In living cells, where a FAP-tagged protein is

NIH-PA Author Manuscript

NIH-PA Author Manuscript

NIH-PA Author Manuscript

present in multiple compartments, it may be difficult to obtain quantitatively informative images due to heterogeneities in intracellular dye concentration or access of the dye to the target sites within cellular structures. Additional studies in our lab are underway to establish relative access of the MG-ester fluorogen dye to FAPs expressed in various subcellular compartments.

Three intracellular-functional malachite green binding FAP clones were prepared as actin fusion constructs, and retrovirally transduced into HeLa cells. We evaluate the brightness of FAP clones labeling the actin cytoskeleton in order to determine the optimal clone for cellular superresolution imaging. This clone (dH6.2) is then used to demonstrate the superresolution imaging approach in fixed and living cells. We demonstrate the control of labeling density in fixed cells using low concentrations of dye, and describe the imaging protocol used to obtain optimal images. We further show improvements in resolution obtained relative to diffraction limited actin images in saponin-treated phalloidin stained cells, and in live, non-permeabilized cells labeled with the MG-ester dye. Together, these studies show that equilibrium association between fluorogenic dyes and FAPs can be used for genetically encoded superresolution imaging by Binding Activated Localization Microscopy (F-BALM).

Results and Discussion

Evaluation of MG-FAP-Actin clones

Three distinct MG-binding clones were derived from the parent MG-binding FAPs through random and targeted mutagenesis efforts, producing clones that retained functional fluorogen activation in the reducing environment of the cells.[40, 41, 43, 49] These proteins were expressed as fusion constructs with the human β-actin gene and retrovirally transduced into HeLa cells using the pQCXIP retroviral system (Clontech). These stable cells were labeled with 100 nM MG-ester dye, revealing clear actin structures in the cells by confocal microscopy (Figure 2). The cells had significant differences in signal level, with the dH6.2 producing the highest signal across numerous independent experiments. Qualitatively, the intracellular signal observed in these cells was consistently dH6.2 > dL5** >> HL4-p13. On this basis, the dH6.2 clone was evaluated further for superresolution imaging using F-BALM. Over a range of laser powers, we were able to achieve localization precision between 10 and 45 nm, which is comparable to other superresolution imaging probes.[50] Importantly, the dH6-fluorgen complex was bright enough at lower laser powers to allow localization imaging of live cells without excessive light exposure. Figures 2 B and C show the distribution of photons and localization precision, respectively, for the dH6.2 clone using a 633 nm laser at 0.4 kW/cm^2.

Influence of dye concentration on labeling density

Localization microscopy requires an optimal labeling density to achieve a sufficient number of localizations in each individual image frame, but to still retain resolvable objects. At low emitter densities, individual objects are rare, and the number of images required to generate a sufficient localization image becomes prohibitive. At high density, however, the likelihood of finding two overlapping objects increases, and these ambiguous localizations are frequently rejected, or subjected to a further round of analysis.[51] Using a fixed cell expressing the dH6.2 FAP-actin construct, we determined the influence of labeling concentration on the density of localizable objects using a single-emitter fitting model. Figure 3A demonstrates the influence of dye concentration on image quality. A low concentration of dye produces an overall low-density image on the structure, and ultimately fails to produce a superresolution image of adequate object density within a reasonable time period (Fig 3A, 80 pM). As the dye concentration is increased, more fits are obtained and

NIH-PA Author Manuscript

NIH-PA Author Manuscript

NIH-PA Author Manuscript

the underlying structure is better resolved (Figure 3A, 480 pM). Fluorogen concentrations above a certain level will result in labeling densities too high to be fit to single emitter models until enough molecules have bleached that single molecule densities are reached (Fig 3B). It is important to note that these high initial labeling conditions are not optimal since the dissociation of dye from bleached complex is slow and the positional information for the bleached molecules is lost. Thus, intermediate concentrations produce more uniformly distributed and still sparse labels, and an increase in the overall density of localized objects is observed. Ultimately, the fine-tuning of dye concentration is critical to optimize imaging reconstructions, yet this is easily achieved through titration of fluorogen at the time of imaging.

To optimize superresolution imaging using F-BALM, we developed a protocol with two unique aspects. The first modification was added to overcome the slow dissociation of the fluorogen. Consistent with this, we observe that the density of localizations decreases over time. This decrease was countered by addition of fresh dye to the milieu during acquisition once the density of objects had fallen to a sufficiently low level. While this was empirically defined, such an approach could be optimized or automated. Secondly, we found that imaging was improved by alternating between light and dark cycles, where an acquisition cycle, typically 20 frames, was followed by 5-10 seconds of “dark” to allow additional binding events to occur. During the dark period, new dye to binds to and accumulates on stable actin filiments, while fits from dye-bound monomeric actin that appear transiently in the TIRF field are not accumulated (Supplementary Online Materials Figure S1 and Supplemental Movie S1). Note that this protocol was used to enhance filamentous actin structures over monomeric actin and therefore, may not be required for other intra-cellular targets. Figure 3C shows a representative superresolution image acquired with F-BALM. Even using this slowed stroboscopic approach, superresolution images on fixed cells were completed within an hour, and typical live cell imaging sessions could proceed for 30 minutes or longer.

Live cell labeling

The cell-permeant MG-ester fluorogen can be used to label living cells as well as fixed cells. The fixed, permeabilized cells are advantageous for high-resolution structure analysis, because the unpolymerized actin monomers are washed away from the sample during the fixation and permeabilization. This process leaves behind only the remaining polymerized actin structures that have incorporated the FAP-actin monomers. In order to image in the living cells, signal that arises from the rapidly diffusing unincorporated FAP-actin monomers is ignored. This is accomplished by exploiting the localization enhancement obtained with immobile proteins. On the timescale of imaging, 100 ms/frame, the rapidly diffusing FAP-actin constructs (D ~10 $\mu m^2/s$) will have a positional variance of 1 μm. This results in blurring of the emitted photons across a greater number of pixels, due to diffusion-mediated variation in the true object location during the exposure. At low labeling densities, there is always a pool of rapidly diffusing unincorporated monomer, which contributes to a cellular background signal (See Supplemental Movie S2). Incorporated FAP-Actin monomers, on the other hand, show very slow diffusion or treadmilling in the actin cytoskeleton, motions that are slow compared to the imaging time. Consequently, their emission is focused into a normal emitter profile, and appears as a more distinct spot with higher peak signal. These differences can be exploited using size and signal thresholds in the analysis, allowing measurement of localized objects even in a modest background of free diffusing emitters.

To provide a direct comparison of underlying actin structure with our F-BALM reconstruction, we introduced Alexa-488-phalloidin into live cells by transient permeabilization with saponin, after which the detergent was removed and the cell allowed

NIH-PA Author Manuscript

NIH-PA Author Manuscript

NIH-PA Author Manuscript

to recover. Addition of phalloidin to the cells stabilized the actin structure and images were acquired for up to 40 minutes at room temperature. Comparison of the superresolution image with the phalloidin labeling shows that the localizations are specific to actin structures (Figure 4A). The profile across identical regions shows a substantial improvement in imaging resolution compared to the widefield phalloidin image (Figure 4B). It is important to note that the FAP labels expressed actin molecules in the cell, while phalloidin selectively labels actin filaments. The localization of some diffusing monomeric actin is responsible for the observed differences between the phalloidin image and the FBALM image. The nonspecific activation of MG-ester on non-expressing HeLa cells does not result in significant background localizations (Supplementary Online Materials Figure S2) , indicating that this is a highly selective fluorogenic label for the expressed tag, even in living cells.

Superresolution imaging of cells at 37° C without the phalloidin-mediated stabilization of actin was also performed in unpermeabilized living cells (Figure 5) over 30 minutes. Under these conditions, we see evidence of dynamic actin rearrangement in the living cell. Although the background of soluble actin reduces the resolvable detail in these images, dynamic extensions of the cell and of filopodia are apparent. The superresolution imaging approach outlined here is practical for both fixed and unperturbed living cells under physiological conditions.

Conclusions

These FAP-fluorogen probes are a useful tool for superresolution imaging. We have shown that these fluorogens can be selectively activated by expressed fluorogen activating proteins in both fixed and living cells, by simple addition of dye to the media, and that superresolution or conventional resolution images can be obtained by using low or high concentrations of dye, respectively. These protein domains can be fused to targets of interest in living cells, providing the first generalizable example of a molecularly specific Binding Activated Localization Microscopy probe.

There are a number of advantages to the use of FAP-fluorogen pairs for localization microscopy. Apart from the added fluorogen dye, there is no particular buffer requirement to achieve the sparse density of emitters. Because these properties derive from equilibrium considerations, and not photochemistry, they are likely to be useful with many distinct FAP-fluorogen pairs in cellular labeling. In addition, the absence of a photoswitching laser can be beneficial for living cells, preventing phototoxicity concerns. Because the FAP-expressing cells are dark until dye is added, future studies would benefit from expression of a spectrally resolved fluorescent protein and FAP fused to the same target, to easily identify expressing cells in a mixed population, and to identify issues related to dye access or loading at different cellular sites.

Multicolor superresolution imaging has proven challenging because cross-talk can arise from aberrant switching or difficulties controlling switching rates of multiple emitters under the same excitation or environmental conditions. Notably, the FAP method provides a new option for orthogonal labeling of cellular targets and the far-red emission of MG can be paired with many other fluorescent proteins or dyes for two-color super-resolution. Serial imaging could then be performed, such that the PALM or STORM label is imaged first, followed by addition of the fluorogen for the second color, eliminating the potential of photobleaching the second color while imaging the first. The ability to independently tune label density by controlling the dye concentration may also prove valuable in this context. Because the optimal density of activated FAP is a function of the underlying biological structure density[52] (i.e. the proximity of labeled molecules in the specimen), the

NIH-PA Author Manuscript

NIH-PA Author Manuscript

NIH-PA Author Manuscript

incorporation of the labeled protein in the structure, and the local concentration of dye in the cell, the required concentration of dye will depend on both the specimen as well as the choice of fluorogen activating protein clone. Importantly, when extended to multiple FAP-fluogen combinations, dye concentrations can be adjusted independently, providing added flexibility compared to multicolor photoswitching probes.

There remains much room for optimization of the FAP-fluorogen pairs that can be used for localization imaging. Multiple dye-protein pairs are available, some of which are highly selective for their cognate dye. These could be tested for function in living cells, allowing tandem (if the colors are different) or serial (if the colors are the same) multiplexing of biological targets. The binding, dissociation and bleaching properties of these FAP-fluorogen pairs are currently being studied in our lab and others, potentially leading to timescale improvements. In addition, the potential for FAP-fluorogen pairs to "recover" after photobleaching has been demonstrated, although not currently with MG-binding fluorogen activating peptides. This property could prove highly valuable for long-term superresolution imaging, where multiple cycles of binding, bleaching and release allow repeated interrogation of the location of a specific protein on timescales where typical bleaching properties of dye-labeled proteins fail.

Finally, these probes may be broadly useful for superresolution imaging, regardless of the selected modality. Our previous studies illustrated that the MG-based FAP-fluorogen pairs could be used for Stimulated Emission Depletion microscopy, resolving actin features down to 110 nm in living cells.[40] Taken with the data presented in this work, we show that cytoplasmic genetically encoded FAPs are a versatile tag that, compatible with live and fixed cells, useful for both STED and localization-based superresolution microscopy.

Experimental Section

FAP-actin vector construction

The FAP fragments were PCR amplified to include a G_4S linker sequence at the 3′ end and cloned into pAcGFP1-actin (Clontech) to replace the GFP using AgeI and BglII. The primers used for PCR amplification are as follows: dH6.2 fw: 5′ ACCGGTATGCAAGTCCAGTTGCAAGAATCTGGA 3′ dH6.2 rv: 5′ AGATCTTGAACCGCCACCTCCGGAGACAGTGACCAGGGTA 3′ dL5** fw: 5′ ACCGGTATGCAGGCCGTCGTTACCCAAGAACCT 3′ dL5** rv: 5′ AGATCTTGAACCGCCACCTCCGGAGAGGACGGTCAGCTGGGTG 3′ HL4.1 fw: 5′ ACCGGTATGCAGGTGCAGCTGGTGGAGTCTG 3′ HL4.1 rv: 5′ AGATCTTGAACCGCCACCTCCTTTGATATCCACTTTGGTCCC 3′ After generating the FAP-actin fusion gene, FAP-actin was cloned into the retroviral vector pQCXIP (Clontech) using AgeI and BamHI. Because HL4.1 contains a BamHI site in its sequence, HL4.1-Actin was PCR-amplified to incorporate AgeI at the 5′ and BclI at the 3′ (BclI shares the same overhang with BamHI). And this PCR fragment was cut with AgeI/BclI and ligated into AgeI/BamHI-digested pQCXIP. Coding sequence of all FAP clones are available as supplemental online materials, and vectors prepared will be deposited in the Addgene repository.

Retroviral packaging and cellular transduction

The packaging cell line GP2-293 cells were co-transfected with pQCXIP-FAP-actin and pVSV-G. The viral supernatant was collected 48 hours post transfection and used to infect the target HeLa cells. The day before infection, $2.5*10^5$ HeLa cells were plated in each well in a 6 well plate. The next day for each well, 1.2 ml viral supernatant and polybrene to a final concentration of 4 μg/ml was added to the cells. Cells were then transferred to 6 cm

NIH-PA Author Manuscript

NIH-PA Author Manuscript

NIH-PA Author Manuscript

and 10 cm dishes for expansion. 0.6 μg/ml and 0.2 μg/ml puromycin (Invitrogen) were used to select and maintain positive cells, respectively.

Confocal microscopy

Cells were imaged using a Carl Zeiss LSM-510 Meta Confocor3 confocal microscope with a 633 nm excitation laser line and a 63X magnification, 1.4 NA objective. Typical laser power was 5%-10% and master gain was ~750. The pinhole was set at 1 Airy unit. Cells were plated in Mattek dishes (MatTek corporation) and imaged in PBS for fixed cells and in OPTI-MEM (Invitrogen) for live cells. 100-200 nM MG-ester was used for FAP-actin staining under all conditions.

Cell Preparation, Fixation and Permeabilization for Localization microscopy

Coverslip treatment: No. 1.5 round (18 mm and 15mm) coverslips (Bioscience Tools) were treated with ddH_2O, acetone, ethanol in an ultrasonic bath for 15 min each and treated with Piranha (70% sulfuric acid and 30% hydrogen peroxide) for 30 min and rinsed extensively with ultra-pure water. Cells were plated in DMEM on the treated coverslips and allowed to adhere from 12-72 hours. For intact cell imaging, cells were washed 3x in 1x PBS and imaged immediately. Otherwise, cells were first pre-extracted using 0.05% saponin in a 10mM MES buffer supplemented with 138mM KCl, 3mM MgCl and 2mM EGTA and in the presence of 1μg/mL Alexa488 Phalloidin (Invitrogen) for 30sec. For live cell imaging cells were very gently washed 6x with 1xPBS and then imaged immediately. For fixed samples, PFA was immediately added to the sample to a final concentration of 4%, and fixed for 15 minutes. Samples were further permeabilized for 5 minutes in 0.05% saponin and rinsed thoroughly and imaged. The cell extraction protocol was modified from Dr. Louise Cramer's free online methods for actin imaging. All imaging (both live cell and fixed cell) was carried out in 1xPBS buffer or DMEM (Gibco) supplemented with 20mM Hepes and 20mM Glucose.

Localization microscopy

F-BALM imaging was performed using an inverted microscope (IX71; Olympus America, Center Valley, PA) equipped with an oil-immersion objective 1.45-NA total internal reflection fluorescence objective (U-APO 150×/NA 1.45; Olympus America). A 637 nm diode laser (HL63133DG, Thorlabs Inc.) was used at between 0.4-0.9kW/cm^2 at the sample for excitation of the FAP bound fluorogen dye and a 488-nm diode laser (Newport Cyan488, 100mW) at 0.03kW/cm^2 or less for Alexa488 Phalloidin excitation. A quad-band dichroic and emission filter set (LF405/488/561/635-A; Semrock, Rochester, NY) set was used for sample illumination and emission. Emission was separated onto different quadrants of an Andor Ixon 897 electron-multiplying charge-coupled device (EM CCD) using a custom built (Thorlabs Inc.) channel splitter with a 561 nm dichroic (Semrock) and a 525/20-25 nm additional emission filter for the Alexa 488. No additional filters were used for the fluorogen. The EM CCD gain was set to 200, and frames were 256 × 256 pixels with a pixel size of 0.106 μm. Where indicated, samples were maintained at 36°C through the use of an objective heater (Bioptechs). Images were acquired as series of 20 frames of 50ms, 100-ms and 200-ms exposures with a ~10 second pause between subsequent acquisitions. This process was automated using custom built software to control laser exposure and camera readout and collected over at least 150 image series (>30minutes total imaging time). Phalloidin co-stained samples were selected before addition of dye based on their phalloidin structure. Nonphalloidin co-stained live cell samples were selected by addition of low levels of dye (80pM). Throughout the acquisition, dye was added as necessary, depending on the number of localization per frame. Over the course of an image series, up to 5nM of dye could be added depending on the FAP-expression level.

NIH-PA Author Manuscript

NIH-PA Author Manuscript

NIH-PA Author Manuscript

Localization analysis and image reconstruction

Data analysis was carried out in a Matlab program developed by Lidke and colleagues.[51, 53] Traditionally in single molecule localization microscopy, the intensity profile of a single emitter was fitted to a 2D-gaussian profile by nonlinear least-squares (NLLS) regression to find the centroid (x,y) of the emitter and the widths of the Gaussian distribution σx and σy. MLE takes the finite camera pixel size, background fluorescence and camera read out noise into consideration, and provides a better estimate of position. A set of parameters are returned through MLE localization including the object position, the intensity and the background count rate. The Cramér-Rao Lower Bound (CRLB) gives the uncertainty of these fitted parameters. The single molecule candidates were identified by applying an intensity threshold filter. Then 7×7 pixel sub-regions including the identified regions were packaged and input to an iterative routine, based on a graphics processing unit (GPU), which allows for a parallelized processing approach and therefore real-time data analysis. The final super-resolution images were generated by adding bivariate 2-D Gaussian blobs at the location of the position estimates. Emitters identified as the same particle in subsequent frames were combined using a using a weighted average taking into account the localization precision in each frame. The sample chamber was mounted in a three-dimensional piezostage (Nano-LPS; Mad City Labs, Madison, WI) with a resolution along the *xyz*-axes of 0.2 nm. No significant sample movement was seen over the imaging time frame, as determined by an image overlay of reconstructions over time. To compare phalloidin low resolution images to F-BALM images, an iterative, gradient-based registration algorithm using the Matlab toolkit DIPimage (TU Delft) was used for image registration and overlay[46] based on the final F-BALM image, and a sum projection of the corresponding phalloidin image.

Supplementary Material

Refer to Web version on PubMed Central for supplementary material.

Acknowledgments

This work was supported in part by grants from the National Institutes of Health and National Science Foundation. The authors would like to acknowledge the following grants for support of various aspects of this research: NIH R01GM100114 (DSL); NSF CAREER Award #0954836 (KAL); 1R01GM086237 (MPB); 8U54GM103529 (QY, CSG, DSL, KAL, MPB) and the New Mexico Spatiotemporal Modeling Center (P50GM0852673). SLS was additionally supported by NSMS IGERT fellowship. The authors would like to thank Dr. Heather Ward for useful discussions regarding phalloidin labeling in live cells.

References Cited

[1]. Hell SW. Nat Methods. 2009; 6:24–32. [PubMed: 19116611]

[2]. Gustafsson MG. J Microsc. 2000; 198:82–87. [PubMed: 10810003]

[3]. Gustafsson MG. Proc Natl Acad Sci U S A. 2005; 102:13081–13086. [PubMed: 16141335]

[4]. Gustafsson MG, Shao L, Carlton PM, Wang CJ, Golubovskaya IN, Cande WZ, Agard DA, Sedat JW. Biophys J. 2008; 94:4957–4970. [PubMed: 18326650]

[5]. Klar TA, Jakobs S, Dyba M, Egner A, Hell SW. Proc Natl Acad Sci U S A. 2000; 97:8206–8210. [PubMed: 10899992]

[6]. Klar TA, Engel E, Hell SW. Phys Rev E Stat Nonlin Soft Matter Phys. 2001; 64:066613. [PubMed: 11736302]

[7]. Han KY, Willig KI, Rittweger E, Jelezko F, Eggeling C, Hell SW. Nano Lett. 2009; 9:3323–3329. [PubMed: 19634862]

[8]. Lidke K, Rieger B, Jovin T, Heintzmann R. Opt Express. 2005; 13:7052–7062. [PubMed: 19498727]

NIH-PA Author Manuscript

NIH-PA Author Manuscript

NIH-PA Author Manuscript

[9]. Betzig E, Patterson GH, Sougrat R, Lindwasser OW, Olenych S, Bonifacino JS, Davidson MW, Lippincott-Schwartz J, Hess HF. Science. 2006; 313:1642–1645. [PubMed: 16902090]

[10]. Hess ST, Girirajan TP, Mason MD. Biophys J. 2006; 91:4258–4272. [PubMed: 16980368]

[11]. Rust MJ, Bates M, Zhuang X. Nat Methods. 2006; 3:793–795. [PubMed: 16896339]

[12]. van de Linde S, Endesfelder U, Mukherjee A, Schuttpelz M, Wiebusch G, Wolter S, Heilemann M, Sauer M. Photochem Photobiol Sci. 2009; 8:465–469. [PubMed: 19337659]

[13]. Cremer C, Kaufmann R, Gunkel M, Pres S, Weiland Y, Muller P, Ruckelshausen T, Lemmer P, Geiger F, Degenhard S, Wege C, Lemmermann NA, Holtappels R, Strickfaden H, Hausmann M. Biotechnol J. 2011; 6:1037–1051. [PubMed: 21910256]

[14]. Sharonov A, Hochstrasser RM. Proc Natl Acad Sci U S A. 2006; 103:18911–18916. [PubMed: 17142314]

[15]. Huang B, Jones SA, Brandenburg B, Zhuang X. Nat Methods. 2008; 5:1047–1052. [PubMed: 19029906]

[16]. Pavani SR, Thompson MA, Biteen JS, Lord SJ, Liu N, Twieg RJ, Piestun R, Moerner WE. Proc Natl Acad Sci U S A. 2009; 106:2995–2999. [PubMed: 19211795]

[17]. Juette MF, Gould TJ, Lessard MD, Mlodzianoski MJ, Nagpure BS, Bennett BT, Hess ST, Bewersdorf J. Nat Methods. 2008; 5:527–529. [PubMed: 18469823]

[18]. Shtengel G, Galbraith JA, Galbraith CG, Lippincott-Schwartz J, Gillette JM, Manley S, Sougrat R, Waterman CM, Kanchanawong P, Davidson MW, Fetter RD, Hess HF. Proc Natl Acad Sci U S A. 2009; 106:3125–3130. [PubMed: 19202073]

[19]. Jones SA, Shim SH, He J, Zhuang X. Nat Methods. 2011; 8:499–508. [PubMed: 21552254]

[20]. Bates M, Huang B, Dempsey GT, Zhuang X. Science. 2007; 317:1749–1753. [PubMed: 17702910]

[21]. Shroff H, Galbraith CG, Galbraith JA, Betzig E. Nat Methods. 2008; 5:417–423. [PubMed: 18408726]

[22]. Dertinger T, Heilemann M, Vogel R, Sauer M, Weiss S. Angew Chem Int Ed Engl. 2010; 49:9441–9443. [PubMed: 21031383]

[23]. Dertinger T, Colyer R, Iyer G, Weiss S, Enderlein J. Proc Natl Acad Sci U S A. 2009; 106:22287–22292. [PubMed: 20018714]

[24]. Cox S, Rosten E, Monypenny J, Jovanovic-Talisman T, Burnette DT, Lippincott-Schwartz J, Jones GE, Heintzmann R. Nat Methods. 2012; 9:195–200. [PubMed: 22138825]

[25]. Heilemann M, van de Linde S, Mukherjee A, Sauer M. Angew Chem Int Ed Engl. 2009; 48:6903–6908. [PubMed: 19670280]

[26]. Heilemann M, van de Linde S, Schuttpelz M, Kasper R, Seefeldt B, Mukherjee A, Tinnefeld P, Sauer M. Angew Chem Int Ed Engl. 2008; 47:6172–6176. [PubMed: 18646237]

[27]. Wombacher R, Heidbreder M, van de Linde S, Sheetz MP, Heilemann M, Cornish VW, Sauer M. Nat Methods. 2010; 7:717–719. [PubMed: 20693998]

[28]. Lukinavicius G, Umezawa K, Olivier N, Honigmann A, Yang G, Plass T, Mueller V, Reymond L, Correa IR Jr. Luo ZG, Schultz C, Lemke EA, Heppenstall P, Eggeling C, Manley S, Johnsson K. Nat Chem. 2013; 5:132–139. [PubMed: 23344448]

[29]. Schoen I, Ries J, Klotzsch E, Ewers H, Vogel V. Nano Lett. 2011; 11:4008–4011. [PubMed: 21838238]

[30]. Roeffaers MB, De Cremer G, Libeert J, Ameloot R, Dedecker P, Bons AJ, Buckins M, Martens JA, Sels BF, De Vos DE, Hofkens J. Angew Chem Int Ed Engl. 2009; 48:9285–9289. [PubMed: 19890928]

[31]. Roeffaers MB, Sels BF, Uji IH, De Schryver FC, Jacobs PA, De Vos DE, Hofkens J. Nature. 2006; 439:572–575. [PubMed: 16452976]

[32]. Lee MK, Williams J, Twieg RJ, Rao J, Moerner WE. Chem Sci. 2013; 42:220–225. [PubMed: 23894694]

[33]. Ondrus AE, Lee HL, Iwanaga S, Parsons WH, Andresen BM, Moerner WE, Du Bois J. Chem Biol. 2012; 19:902–912. [PubMed: 22840778]

[34]. Schwering M, Kiel A, Kurz A, Lymperopoulos K, Sprodefeld A, Kramer R, Herten DP. Angew Chem Int Ed Engl. 2011; 50:2940–2945. [PubMed: 21404374]

NIH-PA Author Manuscript

NIH-PA Author Manuscript

NIH-PA Author Manuscript

[35]. Xu J, Chang J, Yan Q, Dertinger T, Bruchez M, Weiss S. J Phys Chem Lett. 2013; 4:2138–2146. [PubMed: 23930154]

[36]. Szent-Gyorgyi C, Schmidt BF, Creeger Y, Fisher GW, Zakel KL, Adler S, Fitzpatrick JA, Woolford CA, Yan Q, Vasilev KV, Berget PB, Bruchez MP, Jarvik JW, Waggoner A. Nat Biotechnol. 2008; 26:235–240. [PubMed: 18157118]

[37]. Grover A, Schmidt BF, Salter RD, Watkins SC, Waggoner AS, Bruchez MP. Angew Chem Int Ed Engl. 2012; 51:4838–4842. [PubMed: 22461279]

[38]. Shruti S, Urban-Ciecko J, Fitzpatrick JA, Brenner R, Bruchez MP, Barth AL. PLoS One. 2012; 7:e33429. [PubMed: 22438928]

[39]. Holleran JP, Glover ML, Peters KW, Bertrand CA, Watkins SC, Jarvik JW, Frizzell RA. Mol Med. 2012; 18:685–696. [PubMed: 22396015]

[40]. Fitzpatrick JA, Yan Q, Sieber JJ, Dyba M, Schwarz U, Szent-Gyorgyi C, Woolford CA, Berget PB, Waggoner AS, Bruchez MP. Bioconjug Chem. 2009; 20:1843–1847. [PubMed: 20976031]

[41]. Yushchenko DA, Zhang M, Yan Q, Waggoner AS, Bruchez MP. Chembiochem. 2012; 13:1564–1568. [PubMed: 22777954]

[42]. Szent-Gyorgyi C, Schmidt BF, Fitzpatrick JA, Bruchez MP. J Am Chem Soc. 2010; 132:11103–11109. [PubMed: 20698676]

[43]. Yates BP, Peck MA, Berget PB. Mol Biotechnol. 2013; 54:829–841. [PubMed: 23242633]

[44]. Ozhalici-Unal H, Pow CL, Marks SA, Jesper LD, Silva GL, Shank NI, Jones EW, Burnette JM 3rd, Berget PB, Armitage BA. J Am Chem Soc. 2008; 130:12620–12621. [PubMed: 18761447]

[45]. Saunders MJ, Szent-Gyorgyi C, Fisher GW, Jarvik JW, Bruchez MP, Waggoner AS. Methods. 2012; 57:308–317. [PubMed: 22366230]

[46]. Fisher GW, Adler SA, Fuhrman MH, Waggoner AS, Bruchez MP, Jarvik JW. J Biomol Screen. 2010; 15:703–709. [PubMed: 20488980]

[47]. Ghaemmaghami S, Huh WK, Bower K, Howson RW, Belle A, Dephoure N, O'Shea EK, Weissman JS. Nature. 2003; 425:737–741. [PubMed: 14562106]

[48]. Akerman KE, Wikstrom MK. FEBS Lett. 1976; 68:191–197. [PubMed: 976474]

[49]. Szent-Gyorgyi C, Stanfield RL, Andreko S, Dempsey A, Ahmed M, Capek S, Waggoner AS, Wilson IA, Bruchez MP. J Mol Biol. 2013

[50]. Dempsey GT, Vaughan JC, Chen KH, Bates M, Zhuang X. Nat Methods. 2011; 8:1027–1036. [PubMed: 22056676]

[51]. Huang F, Schwartz SL, Byars JM, Lidke KA. Biomed Opt Express. 2011; 2:1377–1393. [PubMed: 21559149]

[52]. Nieuwenhuizen RP, Lidke KA, Bates M, Puig DL, Grunwald D, Stallinga S, Rieger B. Nat Methods. 2013; 10:557–562. [PubMed: 23624665]

[53]. Smith CS, Joseph N, Rieger B, Lidke KA. Nat Methods. 2010; 7:373–375. [PubMed: 20364146]

NIH-PA Author Manuscript

NIH-PA Author Manuscript

NIH-PA Author Manuscript

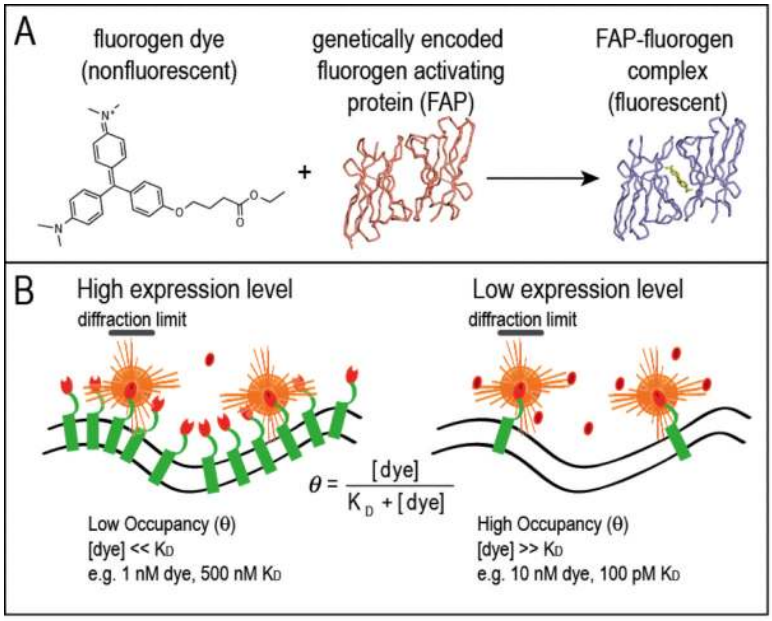

Figure 1.

FAP-Fluorogen detection for single molecule imaging in living cells. A. The FAP-fluorogen pair consists of a non-fluorescent cell-impermeant dye and a genetically encoded protein, which form a fluorescent complex when interacting. B. High abundance proteins can be labeled with low concenrations of dye to acheive sparse molecular labeling (left). Low abundance proteins can be completely labeled and imaged.

NIH-PA Author Manuscript

NIH-PA Author Manuscript

NIH-PA Author Manuscript

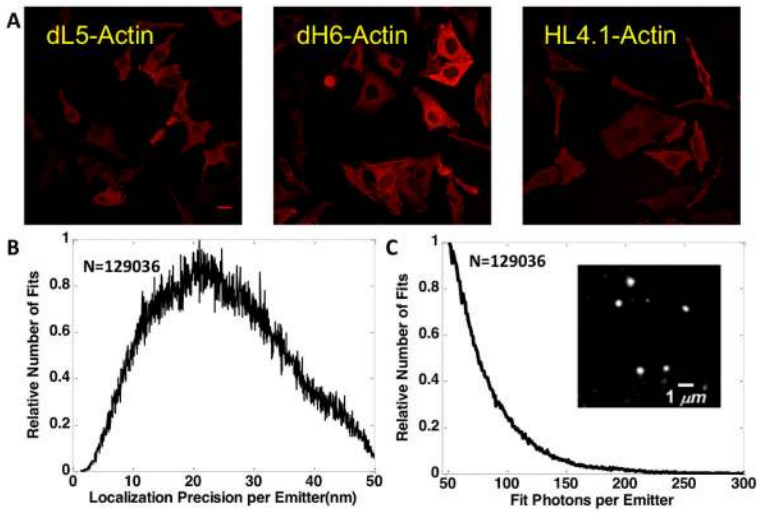

Figure 2.

MG-binding FAPs fused to actin show proper localization and useful superresolution properties. (A) Confocal imaging of various MG-binding FAPs fused to β-actin in live HeLa cells labeled in 100 nM MG-ester dye. Scale-bar 10 μm. (B) the dH6.2-Actin clone shows localization precision typically between 10 an 30 nm per binding event and (C) emitting an average of ~75 detected photons prior to bleaching, producing clearly visible single molecules in each frame (inset).

NIH-PA Author Manuscript

NIH-PA Author Manuscript

NIH-PA Author Manuscript

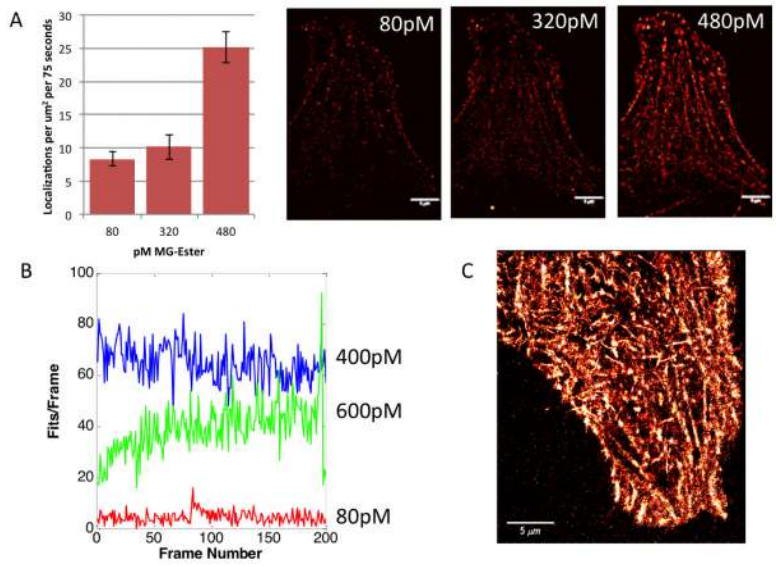

Figure 3.

Influence of dye concentration on localization density. (A) Dye was added at increasing concentration to the same fixed cell, during continuous acquisition revealing improved localization densities at higher dye concentrations, and improved image quality for a reconstruction from a 150 frame subset of the overall acquisition. (B). The influence of dye concentration reveals an optimal level for localization density over time. Higher concentrations require pre-bleaching of the FAPs to achieve resolvable objects, while the lowest concentrations result in low overall object density. (C). Reconstruction of a fixed cell from a 3000 frame acquisition with 173,983 total fits.

NIH-PA Author Manuscript

NIH-PA Author Manuscript

NIH-PA Author Manuscript

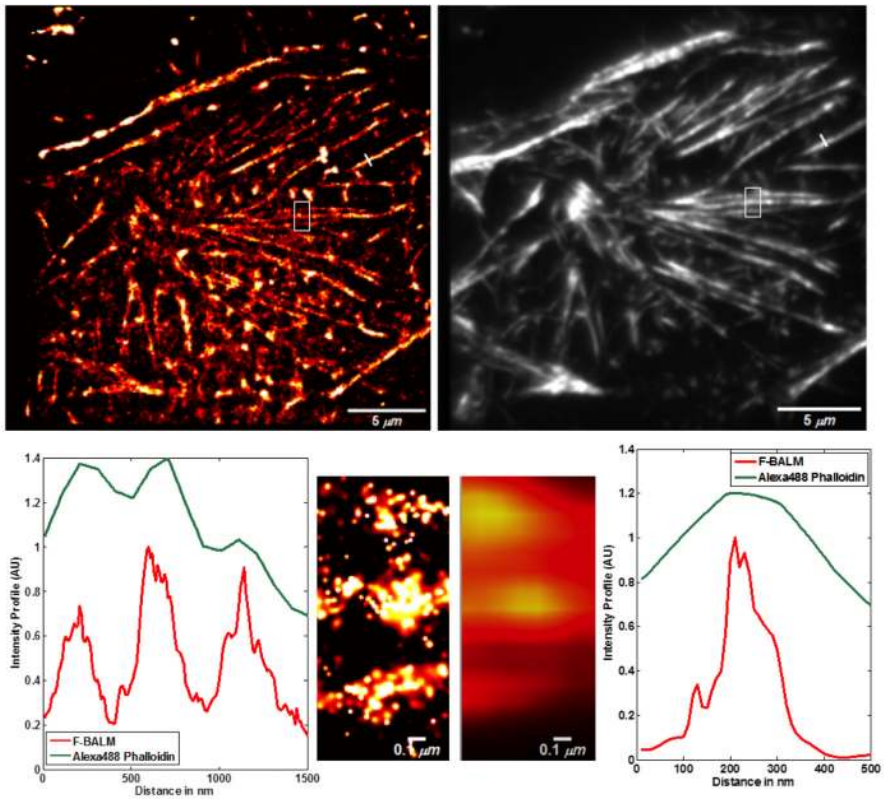

Figure 4.

Live cell F-BALM imaging of actin in HeLa cells. (A) Left shows a reconstruction of FAP-actin while Right shows a wide-field image of phalloidin-Alexa488 obtained simultaneously. (B) cross-section of the boxed region and a line-profile to highlight the improvement in resolution on this structure.

NIH-PA Author Manuscript
NIH-PA Author Manuscript
NIH-PA Author Manuscript

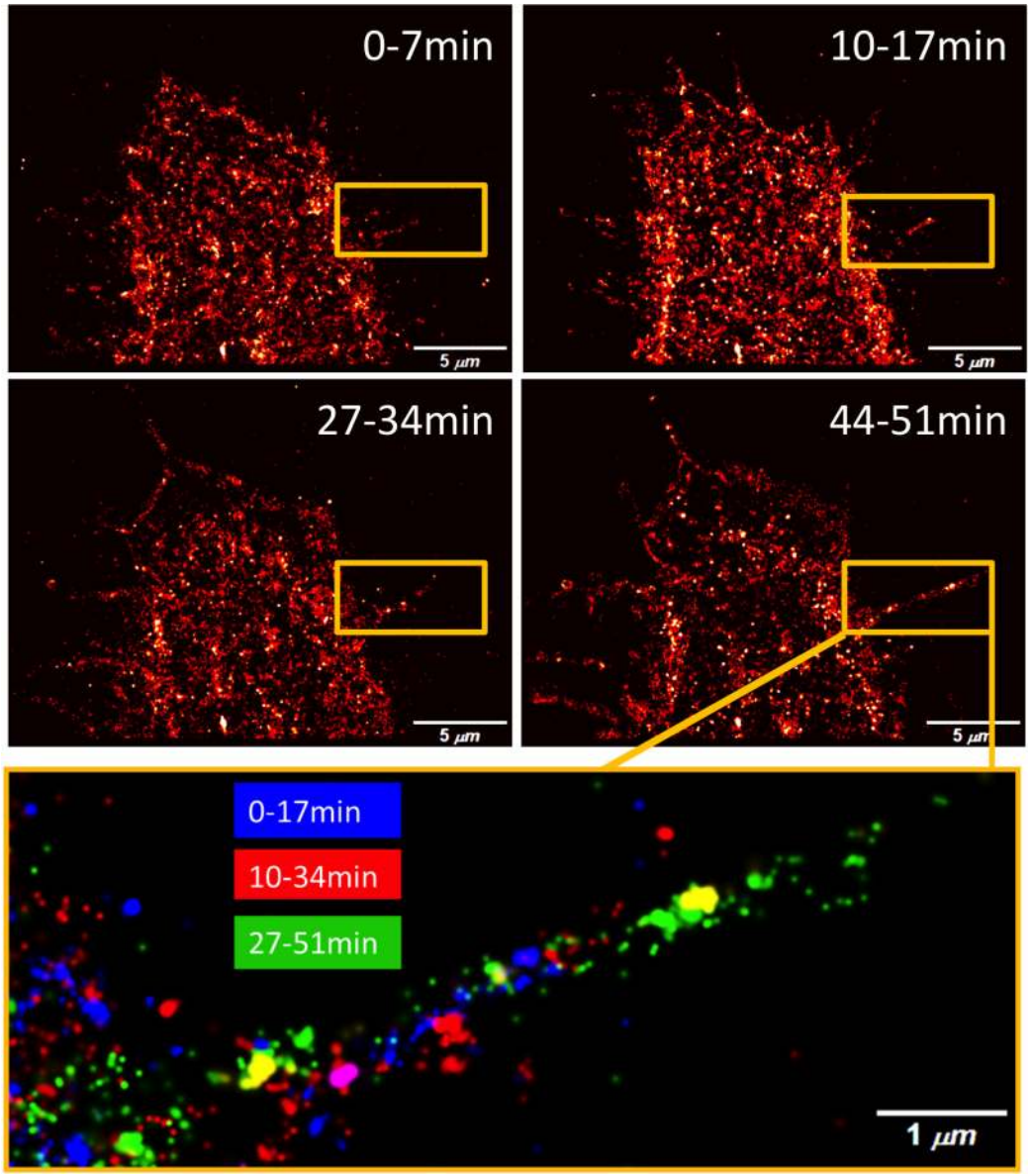

Figure 5.
Imaging of dH6.2-Actin in live Hela cells over a 50 min period. Cells were imaged in DMEM buffered with 20mM Glucose and 20mM HEPES in the presence of 320pM MG-Ester. Snapshots represent reconstructions built from imaging during the time indicated. Colored inset highlights the growth over time of a filipodia structure with each color representing a sliding window accumulated reconstruction over the time frame indicated.